

Terahertz toroidal dipole metamaterial sensors for detection of aflatoxin B1

Jianwei Xu(徐建伟), Shoujian Ouyang(欧阳收剑), Shouxin Duan(段守鑫), Liner Zou(邹林儿), Danni Ye(叶丹妮), Sijia Yang(杨思嘉), and Xiaohua Deng(邓晓华)

Citation: Chin. Phys. B, 2024, 33 (**3**): 038701. DOI: 10.1088/1674-1056/acef02

Journal homepage: http://cpb.iphy.ac.cn; http://iopscience.iop.org/cpb

What follows is a list of articles you may be interested in

Electron beam pumping improves the conversion efficiency of low-frequency photons radiated by perovskite quantum dots

Peng Du(杜鹏), Yining Mu(母一宁), Hang Ren(任航), Idelfonso Tafur Monroy, Yan-Zheng Li(李彦正), Hai-Bo Fan(樊海波), Shuai Wang(王帅), Makram Ibrahim, and Dong Liang(梁栋)
Chin. Phys. B, 2023, 32 (**4**): 048704. DOI: 10.1088/1674-1056/ac8348

Integrated system of traditional THz time-domain spectroscopy and asynchronous optical sampling

Jing Ding(丁晶), Qing-Hao Meng(孟庆昊), Yan Shen(沈妍), Chen-Xin Ding(丁晨鑫), Bo Su(苏波), Hai-Lin Cui(崔海林), and Cun-Lin Zhang(张存林)
Chin. Phys. B, 2023, 32 (**4**): 048702. DOI: 10.1088/1674-1056/ac90b2

Super-resolution reconstruction algorithm for terahertz imaging below diffraction limit

Ying Wang(王莹), Feng Qi(祁峰), Zi-Xu Zhang(张子旭), and Jin-Kuan Wang(汪晋宽)
Chin. Phys. B, 2023, 32 (**3**): 038702. DOI: 10.1088/1674-1056/aca9c7

Scaled radar cross section measurement method for lossy targets via dynamically matching reflection coefficients in THz band

Shuang Pang(逄爽), Yang Zeng(曾旸), Qi Yang(杨琪), Bin Deng(邓彬), and Hong-Qiang Wang(王宏强)
Chin. Phys. B, 2022, 31 (**6**): 068703. DOI: 10.1088/1674-1056/ac474b

Plasmon-induced transparency effect in hybrid terahertz metamaterials with active control and multi-dark modes

Yuting Zhang(张玉婷), Songyi Liu(刘嵩义), Wei Huang(黄巍), Erxiang Dong(董尔翔), Hongyang Li(李洪阳), Xintong Shi(石欣桐), Meng Liu(刘蒙), Wentao Zhang(张文涛), Shan Yin(银珊), and Zhongyue Luo(罗中岳)
Chin. Phys. B, 2022, 31 (**6**): 068702. DOI: 10.1088/1674-1056/ac4f56

Terahertz toroidal dipole metamaterial sensors for detection of aflatoxin B1

Jianwei Xu(徐建伟)[1], Shoujian Ouyang(欧阳收剑)[1], Shouxin Duan(段守鑫)[1], Liner Zou(邹林儿)[1], Danni Ye(叶丹妮)[2,†], Sijia Yang(杨思嘉)[3,‡], and Xiaohua Deng(邓晓华)[3]

[1] *Department of Physics, School of Physics and Materials Science, Nanchang University, Nanchang* 330031, *China*
[2] *Department of Measuring and Controlling Technology and Instrument, Institute of Advanced Manufacturing, Nanchang University, Nanchang* 330031, *China*
[3] *Institute of Space Science and Technology, Nanchang University, Nanchang* 330031, *China*

(Received 13 April 2023; revised manuscript received 28 July 2023; accepted manuscript online 11 August 2023)

Terahertz metamaterial biosensors have attracted significant attention in the biological field due to their advantages of label-free, real-time and *in situ* detection. In this paper, a highly sensitive metamaterial sensor with semi-ring mirror symmetry based on toroidal dipole resonance is designed for a new metamaterial biosensor. It is shown that a refractive index sensitivity of 337.5 GHz per refractive index unit can be achieved under an analyte of saturated thickness near a 1.33 THz transmission dip. For biosensor samples where aflatoxin B1 is dropped on the metamaterial surface in our experiment, dip amplitudes of transmission varying from 0.1904 to 0.203 and 0.2093 are observed as aflatoxin B1 concentrations are altered from 0 to 0.001 μg·ml^{-1} and to 0.01 μg·ml^{-1}, respectively. Furthermore, when aflatoxin B1 concentrations are 0.1 μg·ml^{-1}, 1 μg·ml^{-1}, 10 μg·ml^{-1} and 100 μg·ml^{-1}, dip amplitudes of 0.2179, 0.226, 0.2384 and 0.2527 and dip redshifts of 10.1 GHz, 20.1 GHz, 27.7 GHz and 37.6 GHz are respectively observed. These results illustrate high-sensitivity, label-free detection of aflatoxin B1, enriching the applications of sensors in the terahertz domain.

Keywords: terahertz, metamaterial, toroidal dipole, aflatoxin B1

PACS: 87.50.U–, 78.67.Pt, 87.85.fk **DOI:** 10.1088/1674-1056/acef02

1. Introduction

Terahertz (THz) waves, ranging from 0.1 THz to 10 THz, have attracted much attention since they have significant scientific and technological potential in many fields. In particular, THz biosensing has become a promising tool in biological research due to its label-free, real-time and *in situ* detection advantages.[1–3] Metamaterials exhibit unique electromagnetic characteristics that would not be possible in natural and synthetic materials.[4] So far, the development of metamaterials lies in diverse aspects such as invisibility cloaks,[5] superlenses,[6] filters,[7] modulators[8] and sensors.[9] In particular, metamaterial sensors have attracted much attention due to their small size, ease of integration and excellent performance. Fan and colleagues have done a lot of excellent work in this field.[10–14] For instance, they realized thermal denaturation sensing, concentration sensing and identified types of aqueous solutions of proteins using a flexible twisted dual-layer metamaterial with reflective THz time-domain polarization spectroscopy. They also used an all-dielectric metamaterial with functionalized gold nanoparticles to realize immunosensing of target biomolecules at nanolevel concentrations. Later, they successively used a Pancharatnam–Berry metamaterial sensor and electromagnetically induced transparency (EIT) metamaterial sensor to realize the identification of chiral enantiomers of amino acids. Recently, they have conducted further in-depth research and implemented the recognition of chiral enantiomers of amino acids in an aqueous environment using napole metamaterial sensors. Now, high-sensitivity, real-time monitoring sensing can be realized in metamaterial systems because a high sensitivity and high quality (Q)-factor can be obtained by designing exotic metamaterial structures. For example, metamaterial sensors based on Fano resonance[15–19] and EIT[20–23] were shown to have a sharp resonance that improved performance.[24] Most recently, a new type of metamaterial constructed from toroidal dipole structures was proposed in which coupling between the toroidal dipole and free space is relatively weak, leading to the effective localization of the electromagnetic energy and extreme sensitivity to environmental disturbance.[25–29]

In this paper, mirror symmetric THz metamaterial sensors consisting of periodic toroidal dipole structures are designed. Theoretical analyses and simulations show that the sensitivity and Q-factor can be as high as 337.5 GHz per refractive index unit (RIU) and 26.6, respectively. These values of sensitivity and Q-factor are superior to those of most current metamaterial systems.[30–34] The toroidal dipole sensor is then experimentally fabricated for detection of aflatoxin B1 (AFB1). The results demonstrate that for an analyte of AFB1 solution the minimum measurable concentration can be as low as 0.001 μg·ml^{-1}.

†Corresponding author. E-mail: 862090721@qq.com
‡Corresponding author. E-mail: sjyang@ncu.edu.cn

© 2024 Chinese Physical Society and IOP Publishing Ltd

2. Design and fabrication

A schematic view of the proposed periodic toroidal dipole metamaterial is shown in Fig. 1(a). Here the substrate is polyimide (PI) film with thickness $h_{\rm sub} = 50$ μm, and the permittivity ε and loss tanδ of the PI are set as 3.1 and 0.05, respectively.[35] The unit cell of the toroidal dipole is demonstrated in Fig. 1(b) and consists of two semicircular copper rings with inner diameter $R = 18$ μm and a copper rod with length $L = 54$ μm and width $w = 6$ μm. The gap between the rod and ring, the thickness of the copper structure and the period of the unit cell are $g = 3$ μm, $h = 200$ nm and $P = 70$ μm, respectively. When a THz wave in TE mode (electric field is oriented along y) is vertically incident to the toroidal dipole, as shown in Fig. 1(c), the bilaterally symmetric surface current j can be excited and the loop magnetic field M, which connects head to tail, is confined to a small area. That is, the toroidal dipole vector T is formed in the y direction. We used CST Microwave Studio to simulate the designed structure; all parameters and simulation settings are described in Appendix A.

In our experiment the toroidal dipole metamaterial sample is fabricated as follows. First, the silicon wafer and PI film are successively cleaned by ultrasonic shock with acetone and ethanol. Then, the PI film is pasted onto the silicon wafer using polydimethylsiloxane with a ratio of main to curing agents of 10:1. Then, a 200 nm thick copper film is deposited on the PI film by an electron beam evaporation coating system. Finally, the toroidal dipole metamaterial sample is obtained, as shown in Fig. 1(d), by photolithography and etching.

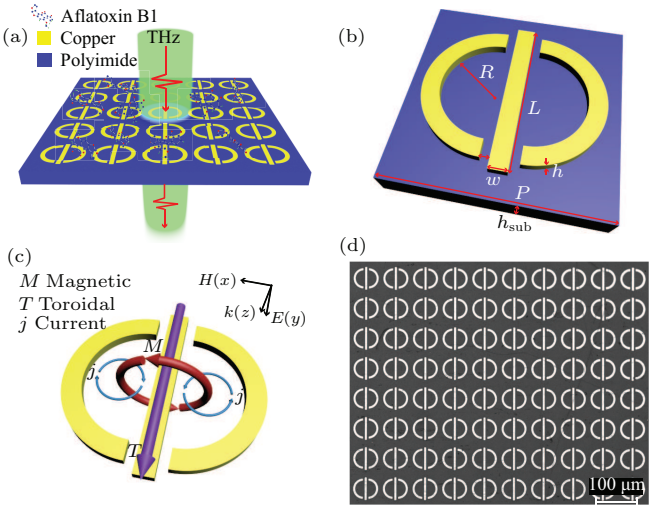


Fig. 1. THz toroidal dipole metamaterial sensor. (a) Schematic diagram of the proposed sensor for AFB1 sensing. (b) Unit cell of toroidal dipole metamaterial with thickness of PI $h_{\rm sub} = 50$ μm, inner diameter $R = 18$ μm, length $L = 54$ μm, width $w = 6$ μm, gap $g = 3$ μm, thickness of copper $h = 200$ nm and period $P = 70$ μm. (c) Diagram of toroidal dipole generation. (d) Microscopic image of metamaterial sample in the experiment.

3. Results and discussion

3.1. Transmission of toroidal dipole metamaterial

The transmission of the toroidal dipole metamaterial by simulation (red curve) and experimental measurement (black curve) is illustrated in Fig. 2(a). The simulation was performed using CST Microwave Studio with normalized TE incidence, and the experimental measurements were made with a THz time-domain spectrometer (THz-TDS). The simulated transmission shows a sharp dip at 1.33 THz and is consistent with the experimental result at 1.3389 THz. To explore the properties of the toroidal dipole in more depth, surface current density and xoz plane magnetic field at 1.33 THz are simulated by CST and demonstrated in Figs. 2(b) and 2(c), respectively. This verifies that the bilaterally symmetric surface current j (Fig. 2(b)) and the loop magnetic field H (Fig. 2(c)) are excited at the resonance dip, The equivalent charges formed at the metal ends of the bilateral symmetrical half rings are respectively recorded as $(q_1, -q_1)$, $(q_3, -q_3)$, and the corresponding electric dipole moments are respectively expressed as P_1 and P_3. The equivalent charge at the end of the middle metal rod is recorded as $(q_2, -q_2)$, and the equivalent electric dipole moment is expressed as P_2, which is opposite to the direction of P_1 and P_3 and suppresses and cancels them. The bilaterally symmetric surface current j can be equivalent to a pair of opposite parallel magnetic dipoles M, which also cancel each other, but they will form a toroidal dipole vector T, as shown in Fig. 1(c), when connected head to tail. The loop magnetic field in Fig. 2(c) also shows that the metamaterial has the characteristics of a toroidal dipole externally at the resonance frequency. In addition, the Q-factor can be defined as $Q = f_0/\text{FWHM}$ to quantitatively describe the sensing performance, where f_0 is the resonance frequency and FWHM is full width at half maximum. Here, $Q = 26.6$ can be obtained at the 1.33 THz resonance dip.

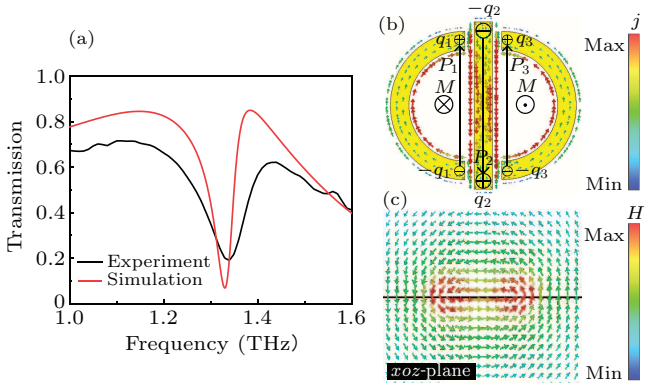


Fig. 2. (a) Simulated and experimental transmission spectra of the toroidal dipole metamaterial. (b) Surface current density j and (c) xoz plane magnetic field vortex H of the toroidal dipole metamaterial at 1.33 THz.

3.2. Biosensor based on the toroidal dipole metamaterial

Based on the properties of the toroidal dipole with sensitivity to geometrical parameters, THz metamaterial biosen-

sors can be designed as shown in Fig. 1(a). Specifically, for a biosensor system with the analyte on the Cu metamaterial, the transmissions of the metamaterial obtained by changing the thickness t of the analyte at fixed refractive index $n = 1.6$ are shown in Fig. 3(a). This shows that the resonance dip occurs at 1.33 THz for $t = 0$ μm. For $t = 3$ μm, 6 μm, 9 μm, 12 μm and 15 μm, the resonance dips have redshifts of 163 GHz, 190 GHz, 200 GHz, 204 GHz and 205 GHz, respectively. In Fig. 3(b), the dependence of those frequency shifts and the fitting on t is illustrated. It shows that when t exceeds 12 μm the resonance frequencies are approximately steady. The transmission of the metamaterial when changing the refractive index n of the analyte from 1 to 1.8, with fixed $t = 12$ μm, is depicted in Fig. 3(c). Compared with 1.33 THz when $n = 1$, the resonance dips also undergo redshifts of $\Delta f = 67$ GHz, 136 GHz, 204 GHz and 269 GHz when refractive index $n = 1.2$, 1.4, 1.6 and 1.8, respectively. In particular, the dependence of Δf on n and its fitting curve is illustrated in Fig. 3(d). Here, Δf has a good linear relationship with n. We note that the sensitivity S can be defined as $S = \Delta f / \Delta n$, where Δn is the variation of refractive index n. Here, $S = 337.5$ GHz/RIU can be obtained for the toroidal dipole structure, implying that it can be used as a highly sensitive refractive index sensor.

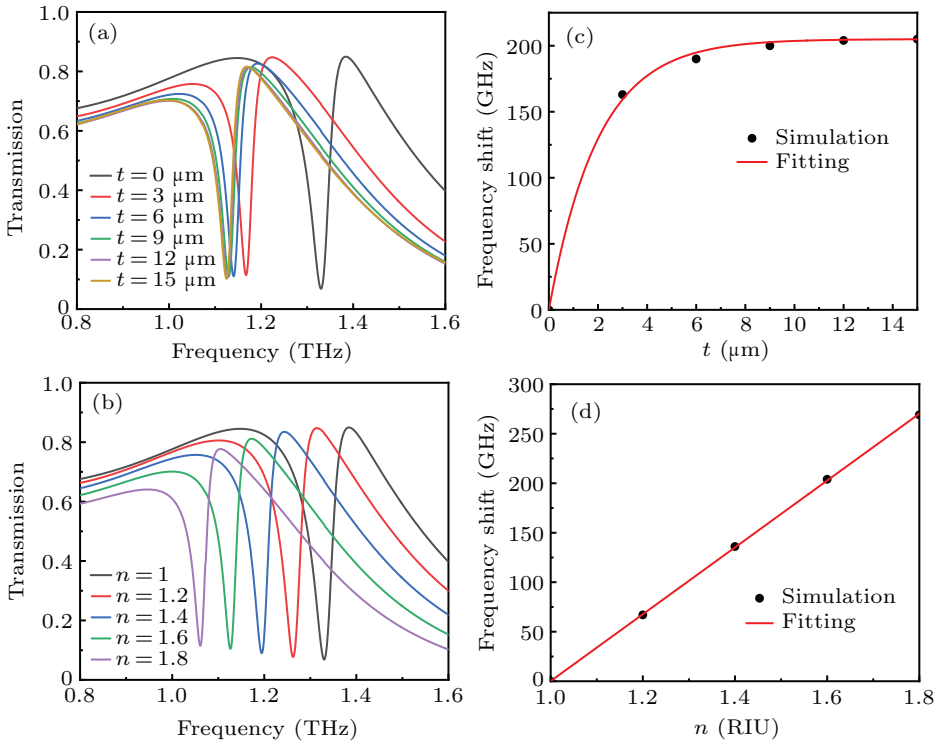


Fig. 3. Biosensor based on the toroidal dipole metamaterial. (a) Transmission and (b) frequency shift of the sensor upon changing the thickness t of the analyte with fixed refractive index $n = 1.6$. (c) Transmissions and (d) frequency shifts obtained by changing the refractive index n of the analyte from 1 to 1.8 with fixed $t = 12$ μm.

3.3. Detection of AFB1 by the toroidal dipole metamaterial

Aflatoxins (AFs) are the most dangerous group of mycotoxins due to their highly toxic, mutagenic, teratogenic and carcinogenic properties.[36] Among the aflatoxins, AFB1 is the most hepatocarcinogenic and hepatotoxic and occurs as a contaminant in a variety of foods.[37] So far, many methods, including traditional high-performance liquid chromatography,[38–40] enzyme-linked immunosorbent assay[41–43] and liquid chromatography coupled to tandem mass spectrometry,[44–46] have been proposed to detect AFB1. However, they are generally time-consuming, require expensive equipment and dangerous chemicals and are labor-intensive. In comparison, detection based on THz metamaterial structures could be quick and convenient. In particular, when different concentrations of AFB1 are dropped on our toroidal dipole metamaterial AFB1 analyte layers of different thicknesses are formed. The higher the concentration of AFB1 solution, the thicker the AFB1 layer. Variations of THz transmission spectra can be observed for highly sensitive sensing. The preparation and detection process for different concentrations of AFB1 solutions are detailed in Appendix B. We further expanded the differences in the AFB1 analyte layer by adding and drying the AFB1 solution three times in the experiment, which can improve the sensitivity and detection limit while reducing the impact of experimental error. This method can also increase the number of samples added according to the actual situation to achieve more sensitive detection.

Figures 4(a) and 4(b) separately show the sample and microscopic image of the toroidal dipole metamaterial with 100 μg·ml^{-1} of AFB1. The transmission and correspond-

ing variations for different AFB1 concentrations are demonstrated in Figs. 4(c) and 4(d), respectively. Here, for very low concentrations, the frequency of the resonance dip shows no distinct change, but its dip amplitude varies. Specifically, when the concentration varies from 0 to 0.001 μg·ml^{-1}, and 0.01 μg·ml^{-1}, the dip amplitudes move from 0.1904 to 0.203, and 0.2093, respectively. For slightly larger concentrations, both resonance frequency and dip amplitude shift. In detail, for AFB1 concentrations of 0.1 μg·ml^{-1}, 1 μg·ml^{-1}, 10 μg·ml^{-1} and 100 μg·ml^{-1}, amplitudes of 0.2179, 0.226, 0.2384 and 0.2527, respectively, and redshifts of 10.1 GHz, 20.1 GHz, 27.7 GHz and 37.6 GHz, respectively, are obtained. By referring to the method of estimating the limit of detection (LOD) in Ref. [47], we determined that the LOD of AFB1 under our experimental conditions was less than 0.001 μg·ml^{-1}, which is lower than the requirement for AFB1 residue of most agricultural products and ensures food safety.

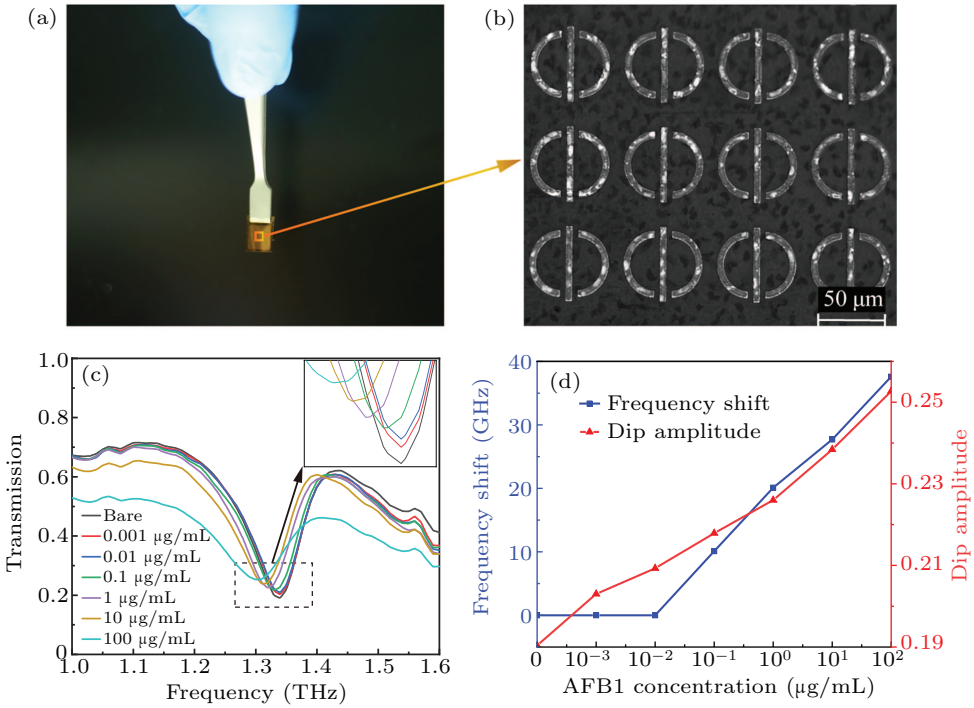


Fig. 4. Detection of AFB1 by the toroidal dipole metamaterial: (a) sample and (b) microscopic images of toroidal dipole metamaterial with drops of 100 μg·ml^{-1} of AFB1. (c) Transmission spectra of toroidal dipole sensors with different concentrations of AFB1. (d) Dependence of frequency shift and amplitude variations of the transmission dips on the concentration of AFB1.

4. Conclusion

A THz metamaterial based on toroidal dipole resonance is explored by simulations and experiment. It is shown that a Q factor of 26.6 and a refractive index sensitivity of 337.5 GHz/RIU can be achieved. For the AFB1 biosensors in our experiment, dip amplitudes of transmission varying from 0.1904 to 0.203 and 0.2093 are observed as AFB1 concentrations are altered from 0 to 0.001 μg·ml^{-1} and 0.01 μg·ml^{-1} respectively. When AFB1 concentrations are 0.1 μg·ml^{-1}, 1 μg·ml^{-1}, 10 μg·ml^{-1}, 100 μg·ml^{-1}, dip amplitudes of 0.2179, 0.226, 0.2384 and 0.2527 and dip redshifts of 10.1 GHz, 20.1 GHz, 27.7 GHz and 37.6 GHz are respectively obtained. AFB1 shows strong absorption of THz waves. In the experiment, the change in transmission spectrum amplitude of metamaterials is mainly caused by the absorption of AFB1, and the redshift of resonant frequency is influenced by the different thicknesses of the analyte layer on the device surface. The experimental results imply that the minimum measurable concentration can be as low as 0.001 μg·ml^{-1}, illustrating high-sensitivity, label-free detection of AFB1 and enriching the applications of sensors in the THz domain.

Appendix A: Finite-element simulations

The designed structure is simulated with CST Microwave Studio. All parameters of the metamaterial structures follow the designed structures, as shown in Fig. 1. We note that in the simulations the electric conductivity of copper is set as $\sigma = 5.8 \times 10^7$ S·m^{-1}. Periodic boundaries were used in the x and y directions; the z direction was set to an open boundary.

Appendix B: AFB1 preparation and detection

The 100 μg·ml^{-1} AFB1 standard solution sample was purchased from Qingdao Lihai Pharmaceutical Packaging Technology Co., Ltd. The AFB1 standard solution was prepared with ethanol at concentrations of 100 μg·ml^{-1}, 10 μg·ml^{-1}, 1 μg·ml^{-1}, 0.1 μg·ml^{-1}, 0.01 μg·ml^{-1} and 0.001 μg·ml^{-1}. Ten microliters of each solution were dropped

on the surface of the toroidal dipole sensors. Subsequently, the samples were dried at room temperature for 3 min. These two steps were repeated three times. The transmission spectra of all samples were measured by a THz-TDS filled with nitrogen.

Acknowledgements

Project supported by the National Natural Science Foundation of China (Grant Nos. 61927813, 61865009, and 12104203) and Jiangxi Provincial Natural Science Foundation (Grant No. 20212ACB201007).

References

[1] Ahmadivand A, Gerislioglu B, Tomitaka A, Manickam P, Kaushik A, Bhansali S, Nair M and Pala N 2018 *Biomed. Opt. Express* **9** 373
[2] Narasimhan V, Siddique R H, Hoffmann M, Kumar S and Choo H 2019 *Nanoscale* **11** 13750
[3] Wang Y G, Zhao Z S, Qin J Y, Liu H, Liu A F and Xu M M 2020 *Talanta* **208** 120469
[4] Wang Y, Cui Z J, Zhang X J, Zhang D C, Zhang X, Zhou T and Wang X 2021 *Acta Phys. Sin.* **70** 301 (in Chinese)
[5] Islam S S, Hasan M M and Faruque M R I 2018 *Appl. Phys. A* **124** 1
[6] Mollae M S M and Simovski C 2019 *Phys. Rev. B* **100** 205426
[7] Ren Z B, Liu R Y, Zhang Y C, Lu H S, Li F Y, Liu Y X, Hong X L and Guo Y 2021 *Opt. Commun.* **497** 127159
[8] Deng G S, Xia T Y, Yang J and Yin Z P 2017 *J. Electromagn Waves Appl.* **31** 2016
[9] Xu W D, Xie L J, Zhu J F, Wang W, Ye Z Z, Ma Y G, Tsai C Y, Chen S M and Ying Y B 2017 *Food Chem.* **218** 330
[10] Liu J, Zhang T R, Tan Z Y, Cheng J R, Chang S J and Fan F 2023 *Opt. Lett.* **48** 440
[11] Shi W N, Fan F, Ma L, Zhang T R, Liu J Y, Cheng J R, Wang X H and Chang S J 2023 *Optics & Laser Technology* **162** 109274
[12] Shi W N, Fan F, Li S S, Zhang Z Y, Liu H L, Wang X H and Chang S J 2022 *Sensors and Actuators B: Chemical* **362** 131777
[13] Zhang Z N, Fan F, Shi W N, Zhang T R and Chang S J 2022 *Biomed. Opt. Express* **13** 209
[14] Shi W N, Fan F, Zhang T R, Liu J Y, Wang X H and Chang S J 2023 *Biomed. Opt. Express* **14** 1096
[15] Wang R D, Xu L, Wang J Y, Sun L, Jiao Y N, Meng Y, Chen S, Chang C and Fan C H 2021 *Nanoscale* **13** 18467
[16] Farmani A, Mir A, Bazgir M and Zarrabi F B 2018 *Physica E* **104** 233
[17] Liu G D, Zhai X, Wang L L, Lin Q, Xia S X, Luo X and Zhao C J 2017 *Plasmonics (Norwell, Mass.)* **13** 15
[18] Zhang B H, Wang L L, Li H J, Zhai X and Xia S X 2016 *Journal of Optics* **18** 65001
[19] Wu C, Khanikaev A B, Adato R, Arju N, Yanik A A, Altug H and Shvets G 2012 *Nat. Mater.* **11** 69
[20] Yu D M, Wang L L, Lin Q, Zhai X, Li H J and Xia S X 2016 *Appl. Phys. Express* **9** 54301
[21] Vafapour Z 2017 *Opt. Commun.* **387** 1
[22] Huang Z, Dai Y Y, Su G X, Yan Z D, Zhan P, Liu F X and Wang Z L 2018 *Plasmonics* **13** 451
[23] Zhang J, Mu N, Liu L H, Xie J H, Feng H, Yao J Q, Chen T N and Zhu W R 2021 *Biosensors and Bioelectronics* **185** 113241
[24] Zhang C B, Xue T J, Zhang J, Liu L H, Xie J H, Wang G M, Yao J Q, Zhu W R and Ye X D 2021 *Nanophotonics* (Berlin, Germany) **11** 101
[25] Ye Q W, Guo L Y, Li M H, Liu Y, Xiao B X and Yang H L 2013 *Phys. Scr.* **88** 55002
[26] Yang S Y, Liu Z, Jin L, Li W X, Zhang S, Li J J and Gu C Z 2017 *ACS Photonics* **4** 2650
[27] Ahmadivand A, Gerislioglu B, Noe G T and Mishra Y K 2019 *ACS Appl. Electron Mater.* **1** 637
[28] Chen X and Fan W H 2019 *J. Phys. D: Appl. Phys.* **52** 485104
[29] Chen X and Fan W H 2017 *Opt. Lett.* **42** 2034
[30] Saadeldin A S, Hameed M F O, Elkaramany E M A and Obayya S S A 2019 *IEEE Sens J.* **19** 7993
[31] Pan W, Yan Y J, Ma Y and Shen D J 2019 *Opt. Commun.* **431** 115
[32] Zhu L, Li H D, Dong L, Zhou W J, Rong M X, Zhang X Z and Guo J 2021 *Opt. Mater. Express* **11** 2109
[33] Xiong Z G, Shang L P, Yang J P, Chen L Y, Guo J, Liu Q C, Danso S A and Li G L 2021 *IEEE Access* **9** 59211
[34] Wang G Q, Zhu F J, Lang T T, Liu J J, Hong Z and Qin J Y 2021 *Nanoscale Res. Lett.* **16** 1
[35] Yan X, Yang M S, Zhang Z, Liang L J, Wei D Q, Wang M, Zhang M J, Wang T, Liu L H, Xie J H and Yao J Q 2019 *Biosens. Bioelectron.* **126** 485
[36] Amate Ferrer C, Unterluggauer H, Fischer R J, Fernández-Alba A R and Masselter S 2010 *Anal. Bioanal. Chem.* **397** 93
[37] Hojnik N, Modic M, Žigon D, Kovač J, Jurov A, Dickenson A, Walsh J L and Cvelbar U 2021 *Plasma Process Polym.* **18** 2000163
[38] Azeez A Z, Hindi M T, Khudiar M M, AL Saadi A S and Khadim N I 2020 *Journal of Food and Pharmaceutical Sciences* **8** 315
[39] Shar Z H, Pirkash O, Shar H H, Sherazi S and Mahesar S A 2020 *Food Addit Contam Part B Surveill* **13** 72
[40] Vitaku E, Smith D T and Njardarson J T 2014 *J. Med. Chem.* **57** 10257
[41] Maggira M, Sakaridis I, Ioannidou M and Samouris G 2022 *Vet. Sci.* **9** 104
[42] Vita V, Franchino C, Iammarino M and De Pace R 2022 *International Journal of Food Science & Technology* **57** 7496
[43] Murshed S A A, Bacha N and Alharazi T 2019 *J. Food Qual.* **2019** 1614502
[44] Yoshida S, Zhang H Y, Takahashi R, Yoshida S, Abiko Y and Toriba A 2022 *J. Chromatogr A* **1678** 463382
[45] Serafimovska T, Stefanovski S, Erler J, Keskovski Z, Stefkov G, Mitevska M, Darkovska Serafimovska M, Balkanov T and Tonic Ribarska J 2021 *Front. Med. (Lausanne)* **8** 759856
[46] Ouakhssase A, Fatini N and Ait A E 2021 *Food Addit Contam Part A Chem Anal Control Expo Risk Assess* **38** 1561
[47] Zhou L, Mao H J, Wu C Y, Tang L, Wu Z H, Sun H, Zhang H L, Zhou H B, Jia C P, Jin Q H, Chen X F and Zhao J L 2017 *Biosensors and Bioelectronics* **87** 701